Controlled cavity QED and single-photon emission using a photonic-crystal waveguide cavity system

Peijun Yao and S. Hughes

Department of Physics, Queen's University, Kingston, Ontario, Canada K7L 3N6
(Received 14 July 2009; revised manuscript received 28 August 2009; published 28 October 2009)

We introduce a photonic crystal waveguide-cavity system for controlling single-photon cavity quantum electrodynamics (QED). Exploiting Bloch mode analysis and medium-dependent Green function techniques we demonstrate that the propagation of single photons can be accurately described analytically for integrated periodic waveguides with little more than four unit cells, including an output coupler. We verify our analytical approach by comparing to rigorous numerical calculations for a range of photonic crystal waveguide lengths. The semiconductor-based nanophotonics system allows one to nanoengineer various regimes of cavity QED with unprecedented control. We demonstrate maximum Purcell factors of greater than 500 and on-chip single-photon beta factors of about 80% efficiency. Both weak and strong-coupling regimes are investigated, and the important role of waveguide length on the output emission spectra is shown for vertically emitted emission and output waveguide emission.

I. INTRODUCTION

Single semiconductor quantum dots (QDs) are promising candidates for single-photon emission applications because of their unique attributes, e.g., large exciton dipole moments, integrability with compact semiconductor cavity systems,[1–5] and compatibility with telecom components. They also facilitate the study of light-matter interactions at a very fundamental level. However, semiconductor QDs suffer from environment-induced decoherence,[6] which can have a detrimental influence on the desired "indistinguishable" and coherent nature of the emitted photons. In the last few years there have been a number of experiments that show that these shortcomings can be largely overcome by increasing the spontaneous emission rate due to the Purcell effect,[7] which is achieved by coupling the QD exciton to a target cavity mode. For example, planar photonic crystal (PC) cavities such as those pioneered by Akahane *et al.*,[8] allow a pronounced modification of the single-photon decay by careful spatial and spectral tuning of an embedded QD exciton.[9]

While new regimes of semiconductor cavity QED are being experimentally realized using photonic nanocavities, one major drawback of the monolithic cavity is that the photons are typically vertically emitted out of the cavity and thus cannot be efficiently collected and manipulated. Moreover, it is against the general vision of *planar integration*, as one ultimately wants to emit the photons on-chip, into a target propagating mode. Compared to regular microcavity systems, PC waveguides have the inherent advantage that they can collect and control the photons on-chip.[10–16] Moreover, enhanced spontaneous emission does not even need a quasi-closed cavity, and *open system cavity QED* can be exploited to achieve photon emission enhancements by appropriate band-gap engineering of the propagation modes.[17–19] Related experiments on PC waveguides have been performed by Viasnoff-Schwoob *et al.*[20] and by Lund-Hansen *et al.*;[21] though only modest Purcell factors were achieved, the waveguide results of Ref. 21 demonstrated that large beta factors can be achieved for emission into an on-chip waveguide

mode. However, several problems remain with long waveguide samples: since slow waveguide modes are required to increase the local density of states (LDOS), then large disorder-induced propagation losses occur[22–24] and the LDOS peak largely broadens;[25] in addition, for on-chip applications, one needs efficient output coupling, which requires a coupler and an output (non-PC) waveguide. Improvements for single-photon gun applications have been proposed[26] using a small section of a PC waveguide that mimics a slow-light mode; although improved single-photon applications were demonstrated, drawbacks of the finite-size PC waveguide include: (*i*) longer waveguides are required to obtain large Purcell factors (>100), and observing the strong-coupling regime would be difficult; (*ii*) lack of tunability and separation of the QD coupling region with the output coupling region; (*iii*) complex Fabry Pérot ripples appear on the LDOS profile, which can be challenging to overcome and engineer; (*iv*) lack of theoretical insight using the known modes of the system, thus requiring a complex three-dimensional (3D) numerical solution, where parameter design sweeps are not practical; (*v*) the waveguide looses many of the benefits of a PC nanocavity, e.g., local tuning and pronounced QD coupling using best-of-breed Q/V_{eff} ratios, where Q is the quality factor and V_{eff} is the effective mode volume of the cavity.

In this work we investigate a hybrid structure for controlled cavity QED, which combines the benefits of finite-size waveguides, on-chip couplers, and PC nanocavities, integrated together on a planar PC chip. Although a rather complicated structure to model and understand, we show that Bloch mode analysis and Green function theory can be applied to derive an intuitive analytical solution to the full scattering geometry. Our medium-dependent quantum optics theory is supported by numerically exact solutions of the 3D Maxwell equations. A schematic of the proposed device is shown in Fig. 1. Similar integrated devices have been built and measured, and we adopt and optimize the coupler design of Banaee *et al.*[27] To facilitate single-photon emission, an excitation laser can either excite the QD coherently or inco-
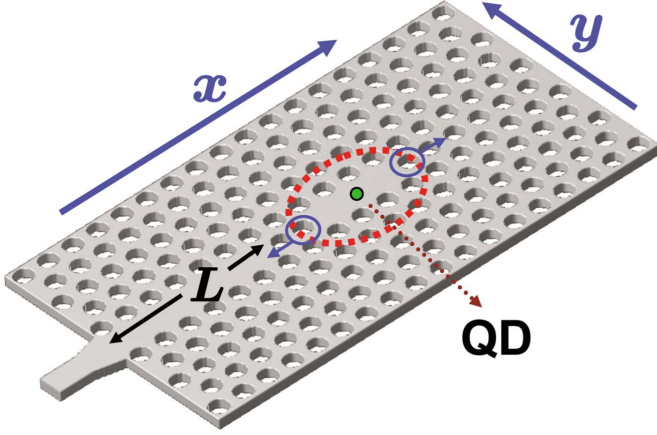
FIG. 1. (Color online) Schematic of the waveguide-cavity single-photon source, which is composed of one cavity, one waveguide, and a QD (indicated by green filled circle, which would nominally be located at the slab center). The PC waveguide length is L. The blue-circled holes are shifted outward to increase the cavity quality factor.

herently. Once excited, the QD exciton will couple to vacuum fluctuations and emit a photon. In the presence of the PC system, this coupling can be controlled in such a way as to, e.g., maximize the probability of photon emission to the left output channel of the waveguide.

II. THEORY

A. Medium Green functions

1. Photonic crystal waveguide plus output waveguide

We first derive the Green function of a PC waveguide coupled to a semi-infinite output waveguide, as shown in Fig. 2, but *excluding* the cavity. The PC waveguide has a finite size L, and the reflection coefficient is unity at the right (perfect PC *without* a cavity), and r at the left. The electric-field eigenmode of this structure in the PC waveguide space ($0 < x < x_0$) is

$$\mathbf{f}_k(r) = \frac{\sqrt{a/L_n}}{1 - re^{2ikL_{\text{eff}}}}[\mathbf{e}_k(r)e^{ik(x-x_0)} + \mathbf{e}_{-k}(r)e^{-ik(x-x_0)}], \quad (1)$$

where a is the pitch, $L_n \to \infty$ is the normalized length of the infinite PC waveguide with eigenmode $e_k(r)$, and L_{eff} is an *effective* optical length that, for the calculations below, is found to be $L_{\text{eff}} \approx L + 0.38a$.[28] The Green function is defined from

$$\left[\nabla \times \nabla \times - \frac{\omega^2}{c^2}\varepsilon(\mathbf{r})\right]\mathbf{G}(\mathbf{r}, \mathbf{r}'; \omega) = \frac{\omega^2}{c^2}\mathbf{1}\delta(\mathbf{r} - \mathbf{r}'), \quad (2)$$

where $\mathbf{1}$ is the unit dyadic and $\varepsilon(\mathbf{r})$ is the dielectric constant for the material, and $\mathbf{G} = \mathbf{G}^T + \mathbf{G}^L$ includes both transverse and longitudinal contributions. The waveguide Green function can be expressed as
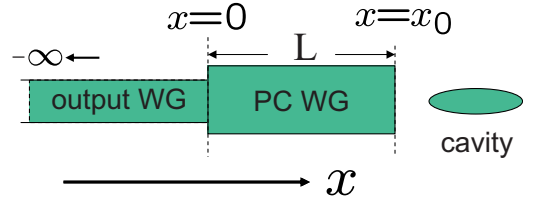

FIG. 2. (Color online) Simple component diagram of the waveguide-cavity system to aid the description of the theoretical formalism; the components include one cavity, one finite-size PC waveguide, and an infinite (or sufficiently long) output target waveguide at the left ($x < 0$).

$$\mathbf{G}_w^T(\mathbf{r}, \mathbf{r}'; \omega) = \sum_k \frac{\omega^2}{\omega_k^2 - \omega^2}\mathbf{f}_k(\mathbf{r}) \otimes \mathbf{f}_k^*(\mathbf{r}'), \quad (3)$$

where $\mathbf{G}_w^T$ is the transverse Green function, and $\otimes$ is the tensor product. Without loss of generality, we assume $k > 0$. Replacing the k summation ($k \equiv k_x$) by an integral, i.e., $\Sigma_k \to \int_{k=0}^{\infty}\frac{L_n}{2\pi}dk$, then

$$\mathbf{G}_w^T(\mathbf{r}, \mathbf{r}'; \omega) = \frac{L_n}{4\pi}\int_0^{\infty} dk\frac{\omega}{\omega_k - \omega - i\delta}\mathbf{f}_k(\mathbf{r}) \otimes \mathbf{f}_k^*(\mathbf{r}'),$$

$$= \frac{L_n}{4\pi v_g}\int_0^{\infty} dk\frac{\omega}{k - k_{\omega} - i\delta}\mathbf{f}_k(\mathbf{r}) \otimes \mathbf{f}_k^*(\mathbf{r}'), \quad (4)$$

where the group velocity $v_g(\omega)$ is treated as positive and δ is a positive infinitesimal variable. Substituting $\mathbf{f}_k$ from Eq. (1) and carrying out the complex integration,

$$\mathbf{G}_w^T(\mathbf{r}, \mathbf{r}'; \omega)\Big|_{0<x'<x_0}^{0<x<x_0} = \frac{ia\omega}{2v_g(1 - 2r\cos(2k_{\omega}L_{\text{eff}}) + r^2)}$$
$$\times [\Theta(x - x')\mathbf{e}_{k_{\omega}}(\mathbf{r}) \otimes \mathbf{e}_{k_{\omega}}^*(\mathbf{r}')e^{ik_{\omega}(x-x')}$$
$$+ \Theta(x' - x)\mathbf{e}_{k_{\omega}}^*(\mathbf{r}) \otimes \mathbf{e}_{k_{\omega}}(\mathbf{r}')e^{-ik_{\omega}(x-x')}$$
$$+ \mathbf{e}_{k_{\omega}}^*(\mathbf{r}) \otimes \mathbf{e}_{k_{\omega}}^*(\mathbf{r}')e^{-ik_{\omega}(x+x'-2x_0)}], \quad (5)$$

and

$$\mathbf{G}_w^T(\mathbf{r}, \mathbf{r}'; \omega)\Big|_{0<x'<x_0}^{x<0} = \frac{iat\omega[\mathbf{f}_{k_{\omega}}^o(y,z)]^* e^{-ik_{\omega}^o x}}{2v_g(1 - 2r\cos(2k\omega L_{\text{eff}}) + r^2)}$$
$$\otimes [\mathbf{e}_{k_{\omega}}(\mathbf{r}')e^{ik_{\omega}x'}$$
$$+ \mathbf{e}_{k_{\omega}}^*(\mathbf{r}')e^{ik_{\omega}(2x_0-x')}], \quad (6)$$

where $\Theta(x - x')$ is the Heaviside function and t is the transmission amplitude of the PC waveguide mode into the output waveguide, which has a propagating mode $\mathbf{f}_{k^o}^o(x,z)e^{ik_{\omega}^o}$, normalized through $\int_{-\infty}^{\infty}\int_{-\infty}^{\infty}dydz\varepsilon(y,z)|\mathbf{f}_{k_{\omega}^o}^o(x,z)|^2 = 1$. Practically, $x < 0$ just means away from the coupler interface, so $x < a$ is typically suffice. In deriving the above equations, we are assuming that the PC waveguide has enough unit cells that a Bloch mode description is valid, and that the waveguide mode is below the light line with a frequency within the

photonic band gap; later, we will quantify these assumptions with rigorous numerical calculations.

2. Adding in the cavity

Next, we add a cavity to the right of the finite waveguide plus output waveguide system (see Fig. 2). As above, all relevant frequencies are assumed to be deep inside the in-plane photonic band gap. The eigenmode of the cavity is $\mathbf{f}_c$ with a resonance frequency ω_c. Note that these values are for the cavity system shown, including perfectly matched layers at the PC waveguide interface (thus no scattering back from the $x = x_0$ interface); the presence of this interface causes a resonance shift and broadening in comparison to a cavity surrounded by an infinite PC. For this waveguide-cavity system, we derive the photon Green function following a similar approach of Cowan and Young,[29] and Hughes and Kamada.[30] Specifically, we expand the transverse Green function $\mathbf{G}_{wc}^T$ of the PC waveguide-cavity system in terms of the cavity and waveguide eigenmodes, $\mathbf{G}_{wc}^T = \Sigma_{\alpha,\beta} B_{\alpha\beta} \mathbf{f}_\alpha \otimes \mathbf{f}_\beta^*$, where $\mathbf{f}_{\alpha/\beta}$ are the transverse eigenmodes of the uncoupled (separate) waveguide and cavity. From the definition of $\mathbf{G}_{wc}^T$, we then obtain a set of equations in matrix form: $\mathbf{MBT} = \mathbf{T}$. The matrix $\mathbf{M}$ has the form

$$\mathbf{M} = \begin{pmatrix} M_{cc} & M_{ck} & \cdots \\ M_{kc} & M_{kk} & \cdots \\ \vdots & \vdots & \ddots \end{pmatrix},$$

with $M_{11} = (\omega_c^2 - \omega^2)/\omega^2$, $M_{ck} = -\langle \mathbf{f}_c | V_c | \mathbf{f}_k \rangle$, and $M_{kk} = (\omega_k^2 - \omega^2)/\omega^2$. The shorthand notation V_c represents the perturbation in the dielectric constant that results from adding in the cavity, else there is a perfect PC (mirror) for $x > x_0$. Without the cavity, then $V = V_w$.

After solving the equation set by matrix inversion, the Green function is obtained analytically for the complete waveguide-cavity system. One obtains

$$\mathbf{G}_{wc}^T \Big|_{x'>0}^{x>0} = \mathbf{G}_w^T + \frac{\omega^2 |\mathbf{f}_c\rangle\langle \mathbf{f}_c|}{\omega_c^2 - \omega^2 - \omega^2 \langle \mathbf{f} | V_c \mathbf{G}_w^T V_c | \mathbf{f}_c \rangle}$$
$$+ \frac{\omega^2 \mathbf{G}_w^T V_c | \mathbf{f}_c\rangle\langle \mathbf{f}_c|}{\omega_c^2 - \omega^2 - \omega^2 \langle \mathbf{f}_c | V_c \mathbf{G}_w^T V_c | \mathbf{f}_c \rangle}$$
$$+ \frac{\omega^2 |\mathbf{f}_c\rangle\langle \mathbf{f}_c | V_c \mathbf{G}_w^T}{\omega_c^2 - \omega^2 - \omega^2 \langle \mathbf{f}_c | V_c \mathbf{G}_w^T V_c | \mathbf{f}_c \rangle}$$
$$+ \frac{\omega^2 \mathbf{G}_w^T V_c | \mathbf{f}_c\rangle\langle \mathbf{f}_c | V_c \mathbf{G}_w^T}{\omega_c^2 - \omega^2 - \omega^2 \langle \mathbf{f}_c | V_c \mathbf{G}_w^T V_c | \mathbf{f}_c \rangle}, \quad (7)$$

where $\mathbf{G}_{wc}^T$ is in operator form, and by spatial projection: $\mathbf{G}_{wc}^T(\mathbf{r},\mathbf{r}') = \langle \mathbf{r} | \mathbf{G}_{wc}^T | \mathbf{r}' \rangle$, $\mathbf{f}_c(\mathbf{r}) = \langle \mathbf{r} | \mathbf{f}_c \rangle$. Thus, the components of $\mathbf{G}_{wc}^T(\mathbf{r},\mathbf{r}')$ projected onto $\mathbf{f}_c(\mathbf{r}) \otimes \mathbf{f}_c^*(\mathbf{r}')$, and onto $\mathbf{f}_k(\mathbf{r}) \otimes \mathbf{f}_c^*(\mathbf{r}')$, are

$$\mathbf{G}_{cc}^T(\mathbf{r},\mathbf{r}';\omega) \Big|_{x'>x_0}^{x>x_0} = \frac{\omega^2 \mathbf{f}_c(\mathbf{r}) \otimes \mathbf{f}_c^*(\mathbf{r}')}{\omega_c^2 - \omega^2 - i\omega(\Gamma_c^0 + \Gamma_{wc})}, \quad (8)$$

and

$$\mathbf{G}_{kc}^T(\mathbf{r},\mathbf{r}';\omega) \Big|_{x'>x_0}^{0<x<x_0} = \frac{ia}{2v_g} \frac{A_{fs}\omega^3 V_{kc} \mathbf{e}_k(\mathbf{r}) e^{ikx} \otimes \mathbf{f}_c^*(\mathbf{r}')}{\omega_c^2 - \omega^2 - i\omega(\Gamma_c^0 + \Gamma_{wc})}, \quad (9)$$

where Γ_c^0 is the vertical decay rate of the cavity, and $\Gamma_{wc} = A_{fs}\Gamma_{wc}^0$ is the coupling coefficient between the finite-size waveguide and the cavity, with $A_{fs}(L_{\mathrm{eff}}, \omega) = 1/[1 + r^2 - 2r\cos(2k_\omega L_{\mathrm{eff}})]$ and $\Gamma_{wc}^0 = \frac{a\omega^2}{v_g}|V_{kc}|^2$; the latter term arises because of the evanescent coupling between the cavity mode and the waveguide mode, where $|V_{kc}|^2 = |V_{ck}|^2 \approx |\int d\mathbf{r} \mathbf{f}_c^*(\mathbf{r}) V_w(\mathbf{r}) \mathbf{e}_k(\mathbf{r}) e^{ikx}|^2$. In practical calculations, and in what follows below, we will compute this coupling exactly using a straightforward numerical simulation. Comparing with the side-coupling waveguide-cavity system,[18] we highlight two important differences: the expression for Γ_{wc}^0 is *doubled* with *unidirectional* coupling (for a side-coupled cavity, $\Gamma_{wc}^0 = \frac{a\omega^2}{2v_g}|V_{kc}|^2$), and there is a finite-size-dependent coupling factor A_{fs}.

The Green function that describes propagation from the dot ($\mathbf{r}' = \mathbf{r}_d$) to the output waveguide is

$$\mathbf{G}_{kc}^T(\mathbf{r},\mathbf{r}';\omega) \Big|_{x'>x_0}^{x<0} = \frac{iat}{2v_g} \frac{A_{fs}\omega^3 V_{kc} \mathbf{f}_k^o(y,z) e^{ik^o x} \otimes \mathbf{f}_c^*(\mathbf{r}')}{\omega_c^2 - \omega^2 - i\omega(\Gamma_c^0 + \Gamma_{wc})}. \quad (10)$$

B. Enhanced spontaneous emission regime

We assume small strongly-confined QDs and invoke the electric-dipole approximation to derive the medium-dependent spontaneous emission rate, or *Einstein A coefficient*, defined through

$$\Gamma(\mathbf{r}_d,\omega_d) = \frac{2\mathbf{d} \cdot \mathrm{Im}[\mathbf{G}^T(\mathbf{r}_d,\mathbf{r}_d;\omega_d)] \cdot \mathbf{d}}{\hbar\varepsilon_0}, \quad (11)$$

where $\mathbf{d} = \mathbf{n}_d d$ is the optical dipole moment of the photon emitter's electronic resonance and $\mathbf{r}_d$ is the spatial position of the QD. Therefore, the enhancement of spontaneous emission rate, i.e., the Purcell factor, can be expressed analytically via $F = \Gamma/\Gamma_h$, where Γ_h is the spontaneous emission rate in a corresponding homogeneous medium. It is noted that the concept of spontaneous emission *rate* only makes sense for weak and intermediate coupling regimes. In other words the application of *Fermi's Golden Rule* assumes the weak-coupling regime, which is an assumption that must be used with care for this system. However, our formalism is not restricted to this regime, and strong-coupling effects will also be investigated later. Using the derived Green functions [Eqs. (8) and (10)], then the on-resonance Purcell factor,

$$F(L_{\mathrm{eff}}, \omega_d = \omega_c) = \frac{\Gamma}{\Gamma_h} = \frac{6\pi c^3 |\mathbf{n}_d \cdot \mathbf{f}_c(\mathbf{r}_d)|^2}{w^2 \sqrt{\varepsilon_b}(\Gamma_c^0 + A_{fs}\Gamma_{wc}^0)}, \quad (12)$$

and the on-resonance beta factor,

$$\beta(L_{\text{eff}}, \omega_d = \omega_c) = \frac{\Gamma_{\text{target}}}{\Gamma_{\text{target}} + \Gamma_{\text{others}}},$$

$$= \frac{\int_{s_o} \text{Re}\{[\mathbf{G}_{kc}^T(\mathbf{r}, \mathbf{r}_d; \omega_c) \cdot \mathbf{n}_d] \times [\boldsymbol{\nabla} \times (\mathbf{G}_{kc}^T(\mathbf{r}, \mathbf{r}_d; \omega_c) \cdot \mathbf{n}_d)]^*\} \cdot d\mathbf{s}}{\int_{s_d} \text{Re}\{[\mathbf{G}_{cc}^T(\mathbf{r}, \mathbf{r}_d; \omega_c) \cdot \mathbf{n}_d] \times [\boldsymbol{\nabla} \times (\mathbf{G}_{kc}^T(\mathbf{r}, \mathbf{r}_d; \omega_c) \cdot \mathbf{n}_d)]^*\} \cdot d\mathbf{s}}$$

$$= A_{fs}(L_{\text{eff}}, \omega_c) B_{\text{coup}},$$

(13)

where B_{coup} depends on the coupling into the target waveguide, and is determined from the full numerical simulation of a polarization dipole, including the coupler region; s_o and s_d refer to surfaces perpendicular to the output propagating waveguide (at $x < 0$) and to a surface surrounding the dipole, respectively. The target output mode represents the output waveguide, and we have neglected the influence of nonradiative decay since we are considering QD coupling regimes at low temperature in an enhanced emission regime. These analytical formulas are valid for well-defined PC waveguides, and as we will show below, can even be used to accurately describe emission for integrated systems with only four unit cells in the PC waveguide section.

C. Emitted spectra and the strong coupling regime

Assuming an *incoherently* excited QD in vacuum, the exact electric-field operator can be written as[31]

$$\hat{\mathbf{E}}(\mathbf{R}, \omega) = \frac{1}{\varepsilon_0} \mathbf{G}^T(\mathbf{R}, \mathbf{r}_d; \omega) \cdot \mathbf{d}[\hat{\sigma}^-(\omega) + \hat{\sigma}^+(\omega)], \quad (14)$$

where $\hat{\sigma}^{(\pm)}$ are the Pauli operators of the electron-hole pair (exciton). The spectrum, detected at position $\mathbf{R}$, is[31]

$$S(\mathbf{R}, \omega) = |\mathbf{G}^T(\mathbf{R}, \mathbf{r}_d; \omega) \cdot \mathbf{d}|^2$$

$$\times \left| \frac{\alpha_0(\omega)}{(1 - \alpha_0(\omega)\mathbf{n}_d \cdot \mathbf{G}_{cc}^T(\mathbf{r}_d, \mathbf{r}_d; \omega) \cdot \mathbf{n}_d)} \right|^2, \quad (15)$$

where $\alpha_0(\omega) = 2\omega_d d^2 / [\hbar \varepsilon_0 (\omega_d^2 - \omega^2)]$ is the bare polarizability, with ω_d as the exciton resonance frequency. It is noted that the divergent contribution to $\text{Re}[\mathbf{G}(\mathbf{r}, \mathbf{r}; \omega)]$ is neglected, since the net consequence of this term merely results in a small vacuum Lamb (frequency) shift which can be thought to exist already in the definition of ω_d. Using $\mathbf{G}_{cc}^T(\mathbf{R}, \mathbf{r}_d; \omega)$ and $\mathbf{G}_{kc}^T(\mathbf{R}, \mathbf{r}_d; \omega)$ from Eqs. (8) and (10), we obtain the spectrum at any relevant spatial point, e.g., above the cavity or along the output waveguide. For example, when the photon is emitted on-chip along the waveguide, then

$$S_{\text{side}}(\mathbf{R}, \omega) \approx |\mathbf{G}_{kc}^T(\mathbf{R}, \mathbf{r}_d; \omega) \cdot \mathbf{d}|^2$$

$$\times \left| \frac{\alpha_0(\omega)}{(1 - \alpha_0(\omega)\mathbf{n}_d \cdot \mathbf{G}_{cc}^T(\mathbf{r}_d, \mathbf{r}_d; \omega) \cdot \mathbf{n}_d)} \right|^2,$$

(16)

and when the photon is emitted vertically, above the cavity

$$S_{\text{vert}}(\mathbf{R}, \omega) \approx |\mathbf{G}_{cc}^T(\mathbf{R}, \mathbf{r}_d; \omega) \cdot \mathbf{d}|^2$$

$$\times \left| \frac{\alpha_0(\omega)}{(1 - \alpha_0(\omega)\mathbf{n}_d \cdot \mathbf{G}_{cc}^T(\mathbf{r}_d, \mathbf{r}_d; \omega) \cdot \mathbf{n}_d)} \right|^2.$$

(17)

We now have all the relevant formulas to compute the Purcell factor, beta factor, and emission spectrum for the integrated waveguide-cavity system shown in Fig. 1.

III. CALCULATIONS

A. Weak coupling regime

In order to validate the above Green function theory, a direct 3D finite difference time domain (FDTD) calculation of the Green function terms is first performed.[32,33] We use parameters representative of the popular L3 cavity[8] and a nominal W1 (removed row of holes) waveguide, with the following parameters: semiconductor slab dielectric constant $\varepsilon = 12$; the lattice constant is $a = 420$ nm (PC pitch); the two holes as indicated in Fig. 1 are shifted outward by a distance of $0.15a$; the thickness of the slab and radius R of the air holes are $0.5a$ and $0.275a$, respectively; and the width of the output waveguide is 470 nm, which was optimized to give the largest beta factor. The TE (transverse electric)-like band gap ranges from 0.760 to 0.935 eV (corresponding to $0.26 - 0.32 c/a$ in normalized frequency units, or 185 to 228 THz), and the band structure of the waveguide mode is shown in Fig. 3(a). In the frequency range of our interest, the waveguide is single mode and under the light line (gray shaded region). In Fig. 3(b), we show the enhancement of the spontaneous emission versus frequency for a maximally positioned and y-aligned QD exciton, with $L = 6a$; the Purcell factor spectra exhibit a typical Lorentzian line shape that agrees with the analytical expression of Eq. (8). The electric-field distribution at the resonant frequency (indicated by red circle in Fig. 3) is also shown in Fig. 4. The local-field strength in the cavity is pronounced and the energy is mainly guided into the coupled PC waveguide, and subsequently into the target output waveguide; both a significant Purcell factor and an enhanced beta factor are obtained. Although the Purcell factor is reduced in comparison to a bare waveguide, the emphasis here is on achieving an enhanced Purcell factor while still obtaining a large on-chip β factor. These Purcell factors give a quantitative measure of the enhancement in the projected LDOS, and are already large enough, with suitable QD coupling, to facilitate strong coupling. The
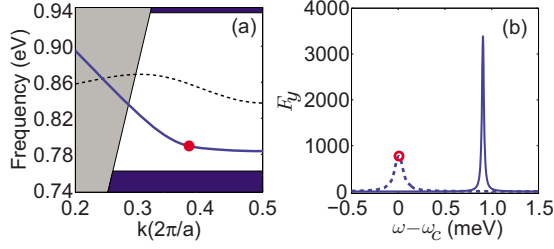
FIG. 3. (Color online) (a) The TE-like band structure of the planar PC (W1) waveguide (see Fig. 1). The filled red dot indicating the waveguide-cavity resonant frequency $\omega_c = 0.79$ eV (~ 192 THz), with a corresponding $k(\omega_c) = 0.75\pi/a$. (b) Theoretical maximum Purcell factors of waveguide-cavity system vs frequency when $L = 6a$ (dashed curve), the resonant frequency is labeled by red circle. For reference, we also show the bare cavity results with the solid curve for a cavity surrounded by a large number of holes on all sides; the frequency shift is a result of the different boundary conditions for the finite-size cavity.

effective mode volume of the cavity system is found to be $V_{\text{eff}} \approx 0.063$ μm^3, which can be related to the cavity mode position at the peak field antinode, through $|\mathbf{f}_c(\mathbf{r}_{\text{antinode}})|^2 = 1/V_{\text{eff}}\varepsilon$.

Next, we carry out a systematic investigation of the Purcell factor as a function of length L, where L is increased by an integer multiple of a. The results are shown in Fig. 5(a), and the data are successfully fitted with the analytical form introduced earlier. The main parameters required for the analytical formulas are extracted from carrying out only one numerical simulation yielding $r = 0.21$ and $\Gamma_c^0/\Gamma_{wc}^0 = 0.31$; the center wave vector $k(\omega_c) = 0.75\pi/a$ is obtained from the band structure. From Fig. 5, we can conclude that when L is larger than $3a$, then the Bloch mode theory becomes valid. Of course, the analytical theory fit is only effective for integer multiple of a because of the coupler dependence of r. If we want to show the case of a continuously varying L, one should first calculate r (and t) for various unit-cell truncations at the output coupler. However, since we have optimized this coupler region, the most practical case is for the integer number of unit cells. Importantly, our calculations include the output reflection coefficient and the length of the waveguide. In addition, one can also tune the properties of the cavity, e.g., to the target exciton resonance, and still overlap with the broadband coupling region of the PC waveguide mode [20–40 meV bandwidth below the light line, c.f. Fig. 3(a)].
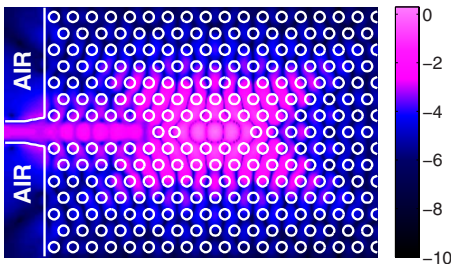

FIG. 4. (Color online) The distribution of electric-field amplitude $[|\mathbf{E}(\omega_c)|]$ at slab center plane on a logarithmic scale.
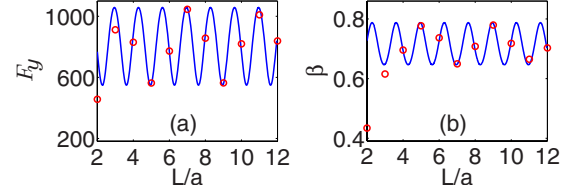

FIG. 5. (Color online) The dependence of (a) Purcell factor and (b) beta factor as a function of waveguide length, L. The data indicated by red circles are obtained from the full 3D numerical simulation, while the blue curves show the results from the derived analytical expression.

As shown in Fig. 5(b), we also investigate the single-photon β factor; this parameter quantifies the efficiency of emitting a single photon into the desired output mode, namely, the waveguide mode after the coupler (c.f. Figs. 1 and 2). The beta factor is first calculated using the FDTD technique by computing the emitted fields at the left of the coupler; these fields are subsequently mode-overlapped with the desired waveguide mode and normalized with respect to the total power flowing out of the lossless device. We first obtain the total emitted power P_t by having six field surface monitors completely surrounding the emitting dipole; we also record the propagation power after the field travels through the coupler P_{out}, and calculate the field distribution $\mathbf{E}_i(\mathbf{r})$ and $\mathbf{H}_i(\mathbf{r})$, including all bound and radiation mode contributions. We then adopt a mode overlap integral technique and calculate the projection of the scattered field that overlaps with the target output waveguide mode. Labeling the electric and magnetic field of the target mode as $\mathbf{E}_{\text{out}}(\mathbf{r})$ and $\mathbf{H}_{\text{out}}(\mathbf{r})$, respectively, then the overlap integral can be expressed as

$$OI = \frac{\text{Re}\left\{ \dfrac{\int [\mathbf{E}_{\text{out}}(\mathbf{r}) \times \mathbf{H}_i^*(\mathbf{r})] \cdot d\mathbf{S} \int [\mathbf{E}_i(\mathbf{r}) \times \mathbf{H}_{\text{out}}^*(\mathbf{r})] \cdot d\mathbf{S}}{\int [\mathbf{E}_{\text{out}}(\mathbf{r}) \times \mathbf{H}_{\text{out}}^*(\mathbf{r})] \cdot d\mathbf{S}} \right\}}{\text{Re}\left\{ \int [\mathbf{E}_i(\mathbf{r}) \times \mathbf{H}_i^*(\mathbf{r})] \cdot d\mathbf{S} \right\}},$$

(18)

where the surface S is on the y-z plane perpendicular to the target waveguide, at the left of the coupler region. The beta factor is then simply $\beta = OI \times P_{\text{out}}/P_t$. We highlight a few advantages of the current structure: (*i*) the Purcell factors, in comparison to a bare finite-size waveguide, are substantially higher when *over coupled* to the cavity, (*ii*) the Purcell factor and beta factor can be controlled in a systematic way, and (*iii*), the conceptual understanding and coupling can be described analytically; to show that this latter point is also true for the beta factor, we have fitted the analytical form with the previous parameters and found good agreement when $L \geq 4a$ [Fig. 5(b)].

B. Strong coupling regime

Finally, we turn our attention to the strong-coupling regime. Since the coupled QD-PC system results in significant LDOS enhancements, we can naturally probe strong cou-
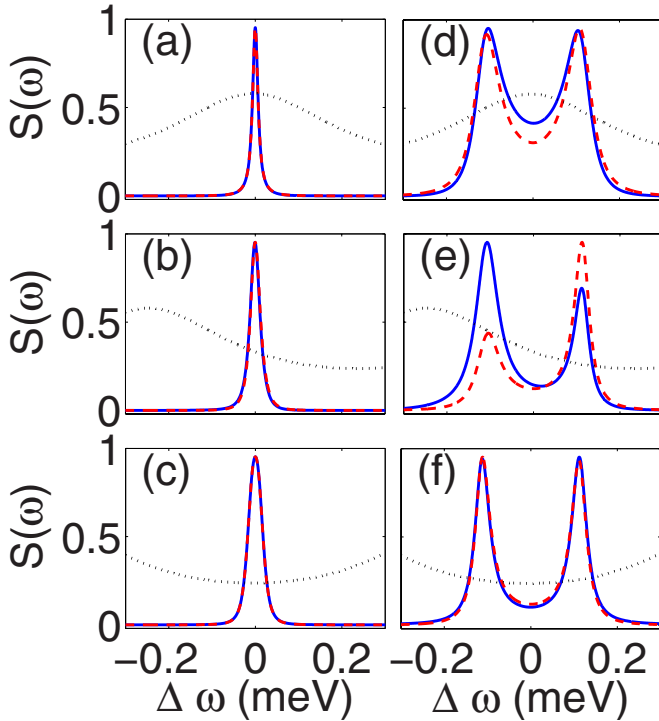
FIG. 6. (Color online) Spectrum emitted vertically from the cavity mode (blue solid curve) and on-chip via the output waveguide mode (red dashed curve); also shown is the finite-size coupling coefficient A_{fs} (black dotted curve). (a–c) d=30 D for L=9a,10a,11a, respectively. (d–f) d=50 D and r=0.21, for L=109a,110a,111a, respectively.

pling and nonperturbative cavity QED either above the cavity or along the output waveguide.

We study emission spectra for detectors that are placed above the cavity and at the output waveguide, for various waveguide lengths. These represent the spectra emitted off-chip and on-chip. For these strong-coupling calculations, one must include the dispersion of the propagating PC waveguide mode; we use a linear dispersion model, $k_\omega = k_{\omega_d} + (\omega - \omega_d)/v_g$, where $v_g(\omega_d) \approx 14$ is obtained from the slope of the waveguide band in Fig. 3(a).

In Figs. 6(a)–6(c), we display the emitted spectra, for a PC waveguide length L=9–10a and a dipole moment of d=30 D (Debye); to ensure maximum coupling, the exciton is resonant with the cavity mode ($\omega_d = \omega_c$). Clearly the spectra, emitted vertically and on-chip are qualitatively different depending upon the PC waveguide length; in particular, one

can see the broadening and thus the Purcell factor increases as we go from (L=9a) to (L=11a), showing that the QD coupling depends sensitively upon the length of the waveguide section. Ideally, for a side-coupled waveguide-cavity system, with no external reflection from the waveguide ends, the shape of spectra emitted vertically from the cavity mode and on-chip via the waveguide mode are symmetric and identical. However, for any real system, the effect of finite size is always there, and in general will result in different spectral shapes for the vertically and horizontally emitted spectra.

We next choose a slightly larger dipole moment of 50 D and a longer PC guide with L=109–111a unit cells. A PC waveguide length of 109–111a has the same peak PF as those with 9–11a, since the length difference between them (100a) is an integer multiple of the period, $8a/3(k_{\omega_d}=0.75\pi/a)$; at the resonance frequency, the Purcell factor is periodic, however for off-resonance it will be more complicated because the field is propagating back and forth between the coupler and the cavity, which appears differently in general for on-chip emission and out-of-plane (vertical) emission [c.f. Eqs. (16) and (17)]. As shown in Figs. 6(d)–6(f), we recognize a significant stronger frequency dependence on the coupling parameter $A_{fs}(L_{\mathrm{eff}}, \omega)$, which can produce significant asymmetries in the emission spectra of a single QD exciton; indeed, there is now a substantial difference between the vertically emitted light and the emitted light on-chip and, in principle, these different spectra could be probed in experiments by placing detectors above the cavity and at the output of the exit waveguide.

IV. CONCLUSIONS

We have theoretically investigated the spontaneous emission properties of an embedded single QD in a photonic crystal waveguide-cavity system. To describe the quantum light-matter interactions in this system, an analytical photon Green function formalism has been developed, which is supported by detailed numerical calculations. The cavity-QED structure can achieve both large Purcell factors and high extraction rates, and allow the investigation of weak and strong-coupling regimes, both on- and off-chip.

ACKNOWLEDGMENTS

[1] E. Moreau, I. Robert, J. M. Gérard, I. Abram, L. Manin, and V. Thierry-Mieg, Appl. Phys. Lett. **79**, 2865 (2001).

[2] C. Santori, D. Fattal, J. Vučković, G. S. Solomon, and Y. Yamamoto, Nature (London) **419**, 594 (2002).

[3] M. Pelton, C. Santori, J. Vučković, B. Zhang, G. S. Solomon, J. Plant, and Y. Yamamoto, Phys. Rev. Lett. **89**, 233602 (2002).

[4] K. Hennessy, A. Badolato, M. Winger, D. Gerace, M. Atatüre, S.

Gulde, S. Fält, E. L. Hu, and A. Imamoğlu, Nature (London) **445**, 896 (2007).

[5] D. Englund, D. Fattal, E. Waks, G. Solomon, B. Zhang, T. Nakaoka, Y. Arakawa, Y. Yamamoto, and J. Vučković, Phys. Rev. Lett. **95**, 013904 (2005).

[6] A. Vagov, V. M. Axt, and T. Kuhn, Phys. Rev. B **66**, 165312 (2002).

[7] E. M. Purcell, Phys. Rev. **69**, 674 (1946).

[8] Y. Akahane, T. Asano, B. Song, and S. Noda, Nature (London) **425**, 944 (2003).

[9] A. Badolato, K. Hennessy, M. Atatüre, J. Dreiser, E. Hu, P. M. Petroff, and A. Imamoğlu, Science **308**, 1158 (2005).

[10] M. Thorhauge, L. H. Frandsen, and P. I. Borel, Opt. Lett. **28**, 1525 (2003).

[11] S. Fan, P. R. Villeneuve, J. D. Joannopoulos, and H. A. Haus, Phys. Rev. Lett. **80**, 960 (1998).

[12] L. Wu, M. Mazilu, J.-F. Gallet, T. F. Krauss, A. Jugessur, and R. M. De La Rue, Opt. Lett. **29**, 1620 (2004).

[13] D. Englund, A. Faraon, B. Zhang, Y. Yamamoto, and J. Vučković, Opt. Express **15**, 5550 (2007).

[14] W. Yao, R.-B. Liu, and L. J. Sham, Phys. Rev. Lett. **95**, 030504 (2005).

[15] J. Gao, F. W. Sun, and C. W. Wong, Appl. Phys. Lett. **93**, 151108 (2008).

[16] X. Yang, M. Yu, D.-L. Kwong, and C. W. Wong, Phys. Rev. Lett. **102**, 173902 (2009).

[17] G. Lecamp, P. Lalanne, and J. P. Hugonin, Phys. Rev. Lett. **99**, 023902 (2007).

[18] S. Hughes, Opt. Lett. **29**, 2659 (2004).

[19] V. S. C. Manga Rao and S. Hughes, Phys. Rev. B **75**, 205437 (2007).

[20] E. Viasnoff-Schwoob, C. Weisbuch, H. Benisty, S. Olivier, S. Varoutsis, I. Robert-Philip, R. Houdré, and C. J. M. Smith, Phys. Rev. Lett. **95**, 183901 (2005).

[21] T. Lund-Hansen, S. Stobbe, B. Julsgaard, H. Thyrrestrup, T. Sünner, M. Kamp, A. Forchel, and P. Lodahl, Phys. Rev. Lett. **101**, 113903 (2008).

[22] S. Hughes, L. Ramunno, J. F. Young, and J. E. Sipe, Phys. Rev. Lett. **94**, 033903 (2005).

[23] M. L. Povinelli, S. G. Johnson, E. Lidorikis, J. D. Joannopoulos, and M. Soljačić, Appl. Phys. Lett. **84**, 3639 (2004).

[24] D. Gerace and L. C. Andreani, Opt. Lett. **29**, 1897 (2004).

[25] D. P. Fussell, S. Hughes, and M. M. Dignam, Phys. Rev. B **78**, 144201 (2008).

[26] V. S. C. Manga Rao and S. Hughes, Phys. Rev. Lett. **99**, 193901 (2007).

[27] M. G. Banaee, A. G. Pattantyus-Abraham, M. W. McCutcheon, G. W. Rieger, and J. F. Young, Appl. Phys. Lett. **90**, 193106 (2007).

[28] Alternatively, one could also define the phase $(2kL+\phi)$ instead of $(2kL_{\text{eff}})$, so L_{eff} incorporates ϕ.

[29] A. R. Cowan and J. F. Young, Phys. Rev. E **68**, 046606 (2003).

[30] S. Hughes and H. Kamada, Phys. Rev. B **70**, 195313 (2004).

[31] S. Hughes and P. Yao, Opt. Express **17**, 3322 (2009).

[32] P. Yao, V. S. C. Manga Rao, and S. Hughes, Laser Photonics Rev. (to be published 2009).

[33] For our FDTD calculations, we have used Lumerical Solition Inc.: see www.lumerical.com.